Inorganic Chemistry

Article

pubs.acs.org/IC

Magnetostructural Correlation for High-Nuclearity Iron(III)/Oxo Complexes and Application to Fe_5, Fe_6, and Fe_8 Clusters

Kylie J. Mitchell, Khalil A. Abboud, and George Christou*

Department of Chemistry, University of Florida, Gainesville, Florida 32611-7200, United States

Ⓢ *Supporting Information*

ABSTRACT: The synthesis and characterization are reported of two new polynuclear Fe^{III} complexes containing the anion of 8-hydroxyquinoline (hqnH), an N,O-chelating ligand. The complexes are $[Fe_8O_4(O_2CPh)_{10}(hqn)_4(OMe)_2]$ (**1**) and $[Fe_6O_2(OH)_2(O_2CPh)_{10}(hqn)_2]$ (**2**) and were obtained from reactions in MeOH (**1**) or H_2O (**2**) using either low-nuclearity preformed clusters or simple metal salts as starting materials. Variable-temperature, solid-state dc and ac magnetic susceptibility studies were carried out and indicate $S = 0$ and $S = 5$ ground states for **1** and **2**, respectively. In order to rationalize the ground states of these and other higher-nuclearity Fe^{III}/O clusters, a magnetostructural correlation (MSC) has been developed specifically for polynuclear Fe^{III}/O systems that predicts the exchange interaction constant (J_{ij}) between two Fe^{III} atoms based on the Fe−O distances and Fe−O−Fe angles at monoatomically bridging ligands. This correlation was refined using selected tri- and tetranuclear complexes in the literature for which both crystal structures and reliable experimentally determined J_{ij} values were available. The predictive capability of the MSC was evaluated by rationalizing the ground-state spins of **1**, **2**, and other Fe_5−Fe_8 clusters, simulating the dc magnetic susceptibility data of polynuclear Fe^{III} complexes, and fitting experimental dc magnetic susceptibility vs T data. The latter fits were evaluated to identify and eliminate systematic errors, and this allowed a protocol to be developed for application of this MSC to other polynuclear Fe^{III}/oxo clusters.

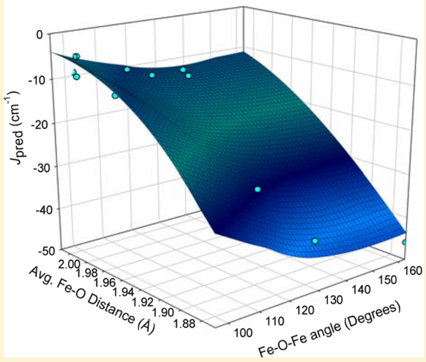

INTRODUCTION

The importance of iron(III)−oxo chemistry to diverse areas such as bioinorganic chemistry and molecular magnetism has led to a wealth of Fe^{III}/oxo cluster chemistry being developed over many years. In the former area, dinuclear compounds have commonly been targeted as synthetic analogues of diiron biomolecules such as hemerythrin,[1] ribonucleotide reductase,[2] methane monooxygenase,[2b,c,3] and others,[4] whereas higher-nuclearity Fe^{III}/oxo clusters have often been sought as potential models of units forming during low Fe-loading levels in the core of ferritin, the intracellular Fe storage protein that sequesters and stores Fe^{III} as a polymeric oxo-hydroxide not dissimilar to ferrihydrite, a hydrous Fe^{III} oxyhydroxide mineral.[5,6] Each ferritin protein can hold up to ∼4500 Fe^{III} ions in this form.[7] The high charge and Lewis acidity of Fe^{III} strongly favor formation of oxide bridges from water molecules and thus foster formation of higher-nuclearity clusters.[8] The latter also have an important impact on the field of molecular magnetism: exchange interactions between oxo-bridged high-spin Fe^{III} ($S = {}^5/_2$) ions are antiferromagnetic (AF), but they can still lead to significant molecular ground state spin values arising from competing exchange interactions (spin frustration) in clusters with high enough nuclearity and the appropriate Fe_x topology containing triangular Fe_3 subunits.[9−11] Spin frustration is defined here in its general sense, most useful to molecular chemists, as the presence of competing exchange interactions of comparable magnitude that prevent (frustrate) the preferred spin alignments,[9,12] thereby often leading to significant uncompensated spin in the ground state. If this ground-state spin value is large enough, the complex can even function as a single-molecule magnet (SMM). SMMs are molecules that below a certain blocking temperature (T_B) exhibit slow magnetization relaxation rates and thus can function as single-domain magnetic particles of nanoscale dimensions.[13]

There is a fundamental desire in Fe^{III}−oxo chemistry, as there is for other metals also, to be able to correlate the exchange interactions between Fe^{III} centers with the structural details and thus be able to predict or rationalize the experimentally determined ground state, the spin energy ladder, and thus the variable-temperature magnetic susceptibility and spectroscopic details. For higher-nuclearity clusters, this would also help one to recognize when spin frustration effects should be expected. For dinuclear compounds, such magnetostructural correlations (MSCs) have been known for many years. The Hatfield and Hodgson MSC for bis-OH^--bridged Cu^{II}_2 complexes is now a classic,[14] correlating the exchange constant (J_{ij}) with the Cu−O−Cu angles, and there have since been a number of related MSCs in dinuclear Cu^{II},[15,16] Ni^{II},[17] Cr^{III},[18] and others.[19,20] This is also true for oxo-bridged dinuclear Fe^{III} complexes, as will be discussed in more detail later (vide infra).[21,22] There are also some useful MSCs for tetranuclear complexes, such as Cu^{II}_4[23] and Ni^{II}_4[24] cubane clusters, for which reliable, experimentally obtained J_{ij} are available.

Received: March 29, 2016
Published: June 13, 2016

ACS Publications © 2016 American Chemical Society

DOI: 10.1021/acs.inorgchem.6b00769
Inorg. Chem. 2016, 55, 6597−6608

However, as the nuclearity of a cluster increases, often with a decrease in the molecular symmetry, the multiple J_{ij} exchange couplings present become much more difficult to determine experimentally, especially for high-spin metal ions such as Fe^{III}. Unfortunately, we have found that the various MSCs developed for dinuclear Fe^{III}_2 compounds are of little or no use for higher-nuclearity clusters. A MSC specially developed for the latter would thus be of tremendous value and utility, either by itself or to complement results of theoretical methods such as DFT, which also become more demanding with increasing metal nuclearity. Given the widespread importance of Fe^{III}/O clusters and the resulting large number of such species being reported, we have decided to target a reliable MSC for this area.

We will first describe the synthesis of two new Fe_x (x = 6 and 8) clusters as part of a long-standing interest in a family of N,O chelates. These clusters were found to possess $S = 0$ and $S = 5$ ground states. In order to help rationalize these ground states, as well as those of so many other Fe^{III}_x/O clusters from our group and others, we shall then describe our development of a new MSC targeted at high-nuclearity Fe^{III}/O clusters, formulated using test clusters in the literature for which both high-quality crystal structures and reliable experimental J_{ij} values have been reported. We shall then show how the MSC can help rationalize experimental ground-state S values and how it can provide reliable starting input values for fits of experimental $\chi_M T$ vs T data. Finally, we shall present a protocol for use of this new MSC.

■ RESULTS AND DISCUSSION

Syntheses. Our group has extensively explored the use of 2-(hydroxymethyl)pyridine (hmpH) in both Fe[25] and Mn[26] chemistry. We have also investigated the use of derivatives of

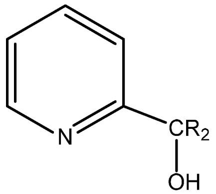

hmpH
(R = H)

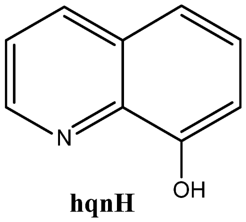

hqnH

hmpH with bulkier groups, R = Me or Ph, on the alcohol arm and have characterized their effect on the nuclearity, symmetry, and magnetic properties of the resulting products.[27] To complete this work, we have explored the use of hqnH to restrict the flexibility of the arm within a second aromatic ring. We have investigated reactions using a variety Fe^{III} starting materials and conditions, and that between preformed $[Fe_3O(O_2CPh)_6(H_2O)_3](NO_3)$, hqnH, and NEt_3 in a 1:1:4 ratio in MeOH yielded a gray precipitate that gave dark red crystals of **1** on recrystallization from CH_2Cl_2/hexanes (eq 1).

$$\begin{aligned}&8[Fe_3O(O_2CPh)_6(H_2O)_3]^+ + 12hqnH + 6MeOH\\&\rightarrow 3[Fe_8O_4(OMe)_2(O_2CPh)_{10}(hqn)_4] + 18PhCO_2H\\&+ 20H_2O + 8H^+ \qquad (1)\end{aligned}$$

The IR spectra of the gray precipitate and dark red crystals were identical. An alternative procedure giving a better yield of **1** of 26% was developed involving the reaction of $Fe(NO_3)_3$ with hqnH, $PhCO_2H$, and NEt_3 in a 2:1:4:6 ratio. Other ratios were also explored but proved inferior in terms of yield and/or purity of **1**. In particular, a Fe^{III}/hqnH ratio of less than 2:1 was found to produce significant amounts of monomeric $Fe(hqn)_3$.[28]

Since **1** contains two bridging MeO^- groups, we explored whether the use of H_2O as solvent might yield analogs with bridging OH^- groups and possibly higher nuclearities. The 1:1 reaction of $[Fe_3O(O_2CPh)_6(H_2O)_3](NO_3)$ with hqnH did indeed yield a OH^--containing product, but it was the lower-nuclearity complex **2** (eq 2).

$$\begin{aligned}&2[Fe_3O(O_2CPh)_6(H_2O)_3]^+ + 2hqnH\\&\rightarrow [Fe_6O_2(OH)_2(O_2CPh)_{10}(hqn)_2] + 2PhCO_2H\\&+ 4H_2O + 2H^+ \qquad (2)\end{aligned}$$

Description of Structures. Complex **1** lies on an inversion center and its structure (Figure 1 and Table 1) contains an $[Fe_8(\mu_3\text{-}O)_4]^{16+}$ core comprising a central $[Fe_2O_2]$ rhombus whose oxide ions (O2, O2′) each connect to a triangular $[Fe_3O]$

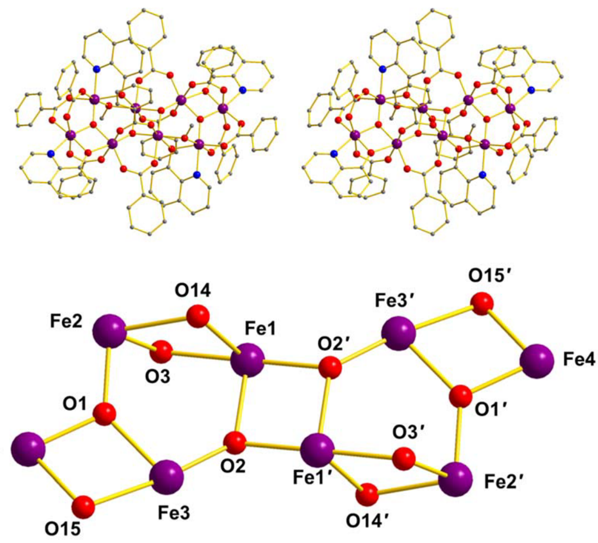

Figure 1. A stereopair of complex **1** and its labeled core; primed and unprimed atoms are related by an inversion center. Color code: Fe^{III}, purple; O, red; N, blue; C, gray. H atoms have been omitted for clarity.

Table 1. Selected Interatomic Distances (Å) and Angles (deg) for 1

Fe1···Fe1′	2.9261(9)	Fe3–O2	1.869(2)
Fe1–O2	1.940(2)	Fe3–O1	1.945(2)
Fe1–O2′	1.974(2)	Fe3–O7	1.997(2)
Fe1–O4	2.012(2)	Fe3–O5	2.044(2)
Fe1–O3	2.022(2)	Fe3–O12	2.059(2)
Fe1–O6	2.082(2)	Fe3–O15	2.187(2)
Fe1–O14	2.102(2)	Fe4–O1	1.868(2)
Fe2–O1	1.844(2)	Fe4–O15	1.990(2)
Fe2–O3′	1.972(2)	Fe4–O9	1.995(2)
Fe2–O8	2.035(2)	Fe4–O11	2.030(2)
Fe2–O14′	2.066(2)	Fe4–O13	2.055(2)
Fe2–O10	2.095(2)	Fe4–N2	2.128(3)
Fe2–N1	2.147(3)		
Fe2–O1–Fe4	120.97(11)	Fe1–O2–Fe1′	96.74(9)
Fe2–O1–Fe3	133.24(11)	Fe2′–O3–Fe1	102.88(9)
Fe4–O1–Fe3	105.07(10)	Fe2′–O14–Fe1	97.07(9)
Fe3–O2–Fe1	119.56(10)	Fe4–O15–Fe3	92.74(9)
Fe3–O2–Fe1′	131.50(11)		

DOI: 10.1021/acs.inorgchem.6b00769
Inorg. Chem. 2016, 55, 6597−6608

unit. Additional monatomic bridges between [Fe_2O_2] and [Fe_3O] units on each side are provided by μ-OMe^- groups (O3, O3′) and μ-OR^- arms of hqn^- chelates (O14, O15, O14′, O15′). The conformation of the two [Fe_3O] units about the bridging [Fe_2O_2] rhombus is anti, in accord with the inversion center. The peripheral ligation is provided by the 4 chelating/bridging hqn^- groups and 10 benzoates in their common syn, syn η^1:η^1:μ-bridging mode.

Complex **1** is similar but not identical to previously reported [$Fe_8O_4(O_2CPh)_{11}(hmp)_5$] and [$Fe_8O_4(O_2CPh)_{12}(hmp)_4$] obtained from the use of hmpH instead of hqnH.[25] The important difference is that **1** contains bridging MeO^- groups in place of some chelate and/or benzoate groups, with corresponding changes to the core structural parameters. We conclude that the use of hqn^- has caused small but distinct differences between **1** and the previous hmp^- clusters, in contrast to the greater differences found when Me- and Ph-substituted hmp^- chelates were employed.[27]

Complex **2** also lies on an inversion center and its structure (Figure 2 and Table 2) contains an [$Fe_6(\mu_3\text{-}O)_2(\mu_2\text{-}OH)_2$]$^{12+}$ core consisting of two triangular [$Fe_3(\mu_3\text{-}O)$] units, similar to those in **1**, joined together at two of their apexes by μ-OH^- ions to give an almost planar Fe_6 unit. The core of **2** can thus reasonably be described as that of **1** without the central [Fe_2O_2] and with some changes to the bridging ligands. Each [Fe(μ-OH^-)Fe] linkage is additionally bridged by two syn,syn μ-benzoates. Also as in **1**, there is an additional monatomic bridge (O3, O3′) in each Fe_3 triangle from the hqn^- groups that chelate Fe2 and Fe2′ and bridge with their alkoxide arms the Fe2Fe3 and Fe2′Fe3′ edges; these monatomic bridges are trans. Peripheral ligation is completed by six additional η^1:η^1:μ-bridging benzoates.

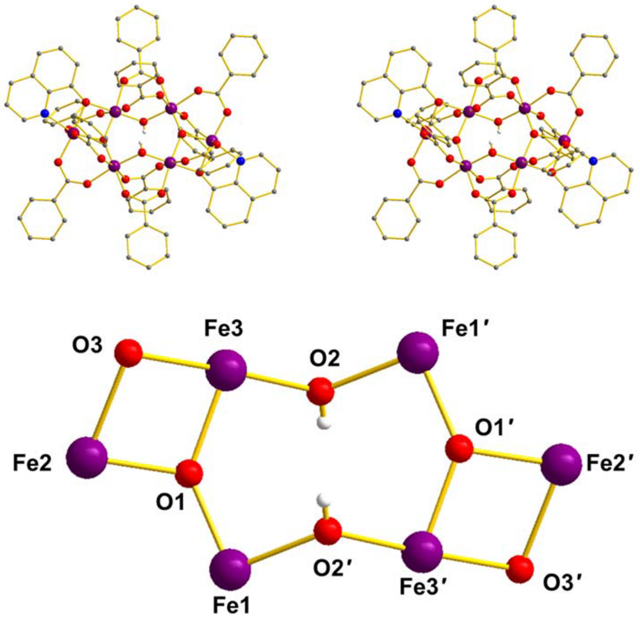

Figure 2. A stereopair of complex **2** and its labeled core; primed and unprimed atoms are related by an inversion center. Color code: Fe^{III}, purple; O, red; N, blue; C, gray; H, white; other H atoms have been omitted for clarity.

Table 2. Selected Interatomic Distances (Å) and Angles (deg) for 2

Fe2···Fe3′	2.9779(5)	Fe2−O12′	2.0405(16)
Fe1−O1	1.8827(15)	Fe2−O3	2.0568(16)
Fe1−O2	1.9716(18)	Fe2−N1	2.145(2)
Fe1−O6	2.0275(16)	Fe3−O2	1.9213(19)
Fe1−O4	2.0314(17)	Fe3−O1′	1.9557(15)
Fe1−O10	2.0422(16)	Fe3−O11	2.0179(16)
Fe1−O8	2.0580(16)	Fe3−O13	2.0199(16)
Fe2−O1	1.8957(15)	Fe3−O3′	2.0430(16)
Fe2−O7	1.9837(16)	Fe3−O9	2.0632(16)
Fe2−O5	2.0237(16)		
Fe1−O1−Fe2	118.16(8)	Fe3−O2−Fe1	123.93(10)
Fe1−O1−Fe3′	136.45(8)	Fe3′−O3−Fe2	93.16(6)
Fe2−O1−Fe3′	101.28(7)		

There have been many reported Fe_6 complexes with a variety of Fe_6 topologies. These have been referred to as (a) planar, (b) twisted-boat, (c) chairlike, (d) parallel triangles, (e) octahedral, (f) fused or extended butterflies, (g) cyclic, and (h) linked-triangles.[29] Such a structural variety has led to many ground-state spin values being determined. Two of these previous Fe_6 complexes, [$Fe_6O_2(OH)_2(O_2CPh)_9(hep)_4$] and [$Fe_6O_2(OH)_2(O_2CPh)_{10}(hep)_2$] ($hep^-$ is the anion of 2-(2-hydroxyethyl)pyridine), have a core related to **2** and have been obtained with either cis or trans disposition of the monatomic oxo bridges;[9] the core of the latter is trans and has an $S = 5$ spin ground state, suggesting a possibly similar ground state for **2** (vide infra).

Magnetic Susceptibility Studies. Solid-state, variable-temperature dc magnetic susceptibility data in the 5.0−300.0 K range in a 0.1 T (1 kG) field were collected on powdered microcrystalline samples of $\mathbf{1}\cdot 3H_2O$ and $\mathbf{2}\cdot 4H_2O$ restrained in eicosane to prevent torquing. For $\mathbf{1}\cdot 3H_2O$, $\chi_M T$ is 8.50 cm^3 K mol^{-1} at 300 K, much smaller than the 35.0 cm^3 K mol^{-1} for eight noninteracting Fe^{III} ions with $g = 2.0$ and indicating antiferromagnetic (AF) exchange interactions, and decreases with decreasing T to 0.60 cm^3 K mol^{-1} at 5.0 K, suggesting an $S = 0$ ground-state spin (Figure 3a). For $\mathbf{2}\cdot 4H_2O$, $\chi_M T$ slowly increases from 11.2 cm^3 K mol^{-1} at 300 K to a maximum of 14.2 cm^3 K mol^{-1} at 25 K and then slightly decreases to 13.7 cm^3 K mol^{-1} at 5.0 K (Figure 3a). The 300 K value is lower than the 26.25 cm^3 K mol^{-1} for six noninteracting Fe^{III} ions with $g = 2.0$, again indicating the presence of AF interactions, but in contrast to $\mathbf{1}\cdot 3H_2O$, the low T data suggest an $S = 5$ ground state: $\chi_M T$ is 10, 15, and 21 cm^3 K mol^{-1} for $S = 4$, 5, and 6, respectively, with $g = 2.0$, as described below.

The $S = 5$ ground state of $\mathbf{2}\cdot 4H_2O$ was confirmed two ways: magnetization (M) data were collected at 1.8−10.0 K in a 0.10−7.0 T dc field (H) and the resulting data were plotted as $M/N\mu_B$ vs H/T (Figure 3b), where N is Avogadro's number and μ_B is the Bohr magneton. The data were fit by diagonalization of the spin Hamiltonian matrix assuming that only the ground state is populated, incorporating axial zero-field splitting ($D\hat{S}_z^{\,2}$) and Zeeman terms, and employing a full powder average. The spin Hamiltonian is given by eq 3

$$\mathcal{H} = D\hat{S}_z^{\,2} + g\mu_B\mu_0\hat{S}\cdot H \qquad (3)$$

where $\hat{S}_z$ is the easy-axis spin operator and μ_0 is the vacuum permeability; the last term is the Zeeman energy associated with the applied dc field. The fit (solid lines in Figure 3b) gave $S = 5$, $g = 1.93(1)$, and $D = 0.31(2)$ cm^{-1}. The excellent fit using data up to 7 T indicates that the ground state is well-isolated (vs kT) from the nearest excited states. A slightly inferior fit was also obtained with $S = 5$, $g = 1.91(1)$, and $D = -0.18(2)$ cm^{-1} [Figure S1, Supporting Information (SI)]. It is common to obtain two acceptable D vs g fits of magnetization

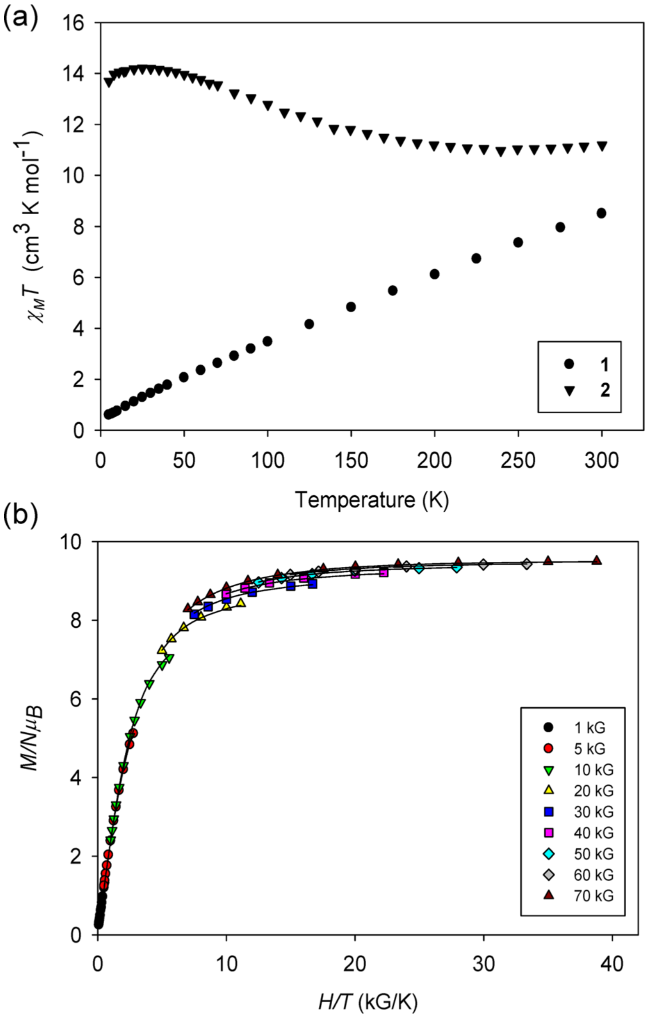

Figure 3. (a) $\chi_M T$ vs T plots for **1**·3H$_2$O and **2**·4H$_2$O in a 0.1 T dc field. (b) Reduced magnetization vs H/T data for **2**·4H$_2$O. The solid lines are the fit; see the text for the fit parameters.

data for a given S value, with $D > 0$ and $D < 0$, since magnetization fits are not very sensitive to the sign of D. More-sensitive techniques such as EPR are required for a more reliable determination of D.

Ac magnetic susceptibility measurements were performed in the 1.8−15 K range using a 3.5 G ac field oscillating at 997 Hz (Figure S2, SI).[30] For **1**·3H$_2$O, the in-phase $\chi'_M T$ decreases from 0.98 cm^3 K mol^{-1} at 15 K to 0.53 cm^3 K mol^{-1} at 1.8 K, confirming an $S = 0$ ground state. For **2**·4H$_2$O, $\chi'_M T$ remains essentially constant down to 7.0 K at ∼14.9 cm^3 K mol^{-1}, consistent with an $S = 5$ ground state, and then slightly decreases to 13.9 cm^3 K mol^{-1} at 1.8 K, assignable to some very weak intermolecular AF interactions. As expected, neither complex exhibited an out-of-phase χ''_M signal (Figure S2, SI).

Magnetostructural Correlation (MSC) for Polynuclear Fe^{III} Clusters. The magnetic properties of polynuclear Fe^{III}/O clusters depend on the exchange interactions, J_{ij}, between Fe atoms, which are dictated by the chemical identity of the bridging ligands and the bridging geometry.[31,32] Exchange interactions can be determined by a variety of means, such as fitting experimental χ_M vs T data for low-nuclearity complexes to the appropriate Van Vleck expression with fit parameters J and an isotropic g,[33,12a] utilization of computational methods such as ZILSH[9,34] or DFT[35] for higher-nuclearity complexes, or simulating or fitting their dc χ_M vs T data using one of the several software packages available that employ matrix diagonalization approaches.[9,36] All these methods, however, become more difficult or near-impossible to employ, or employ reliably, with increasing metal nuclearity. High-nuclearity Fe$^{III}_x$ ($x \geq 6$) complexes become increasingly demanding computationally and/or can lead to many local error minima in simulations or fits of experimental data due to a large number of J_{ij} exchange interactions and often no reliable starting values for them. Therefore, a MSC that relates key structural parameters, such as metal−ligand bond distances and angles, with the sign and magnitude of the pairwise exchange interactions would be extremely useful for rationalizing observed magnetic properties of high-nuclearity complexes with multiple J_{ij}. Further, the predictive capability of such a correlation could greatly aid in providing a reliable starting point for simulations or fits to ensure that conclusions reflecting "reality" are obtained and could even assist in the rational incorporation of favorable structural features to yield desirable magnetic properties.

For such reasons, several groups have reported MSC's in Fe^{III}−O chemistry, primarily for dinuclear Fe^{III} compounds.[21] Gorun and Lippard (GL) investigated dinuclear Fe^{III} complexes bridged by a μ-oxo (O^{2-}, OH$^-$, RO$^-$) and at least one other bridging ligand, plus a very few tri- and tetranuclear ones, and reported an exponential relationship between J and the parameter P (half the shortest superexchange pathway between two Fe^{III} atoms, typically the average Fe−O distance).[21a] The Fe−O−Fe angle was concluded to have only a minor effect on J and was excluded from the model. The authors specifically state that their MSC does not apply to Fe$_2$(μ-O) centers unsupported by other bridging ligands. Weihe and Güdel (WG) also considered singly, doubly, and triply bridged dinuclear Fe^{III} complexes, but with specifically just one *μ-oxide* (O^{2-}) monatomic bridge, and developed an equation for J derived from the angular overlap model (AOM) that depends on both the Fe−O−Fe angle (ϕ) and the Fe−O distance (r) (eq 4).[21b]

$$J_{\text{model}} = (4/25)[e'^{\,2}_{p\pi}(1 + \cos^2\phi) + (e'_{s\sigma} - e'_{p\sigma}(-\cos\phi))^2 + 2e'_{p\sigma}e'_{p\pi}(\sin\phi)^2]f^2(r_1)f^2(r_2) \tag{4}$$

The radial function employed was that in eq 5, where b is a coefficient.

$$f(r)\ \alpha\ \mathrm{e}^{-br} \tag{5}$$

Equation 4 was refined using experimental data for 32 dinuclear complexes to obtain best-fit parameters for each of the AOM ligand field parameters ($e'_{p\pi}$, $e'_{s\sigma}$, $e'_{p\sigma}$) and the b parameter. The final equation simplified to that in eq 6, where $A = 1.337 \times 10^8$ cm^{-1}, $B = 3.536$, $C = 2.488$, and $D = -7.909$ Å^{-1}.

$$J = A(B + C\cos\phi + \cos^2\phi)\exp(Dr) \tag{6}$$

The authors found, at least for the limited range of average Fe−O^{2-} distances (1.77−1.82 Å) in such complexes, that the magnitude of J decreases when the Fe−O^{2-} distance increases at a fixed Fe−O−Fe angle or when the Fe−O−Fe angle increases at a fixed Fe−O^{2-} distance; the Fe−O−Fe angle dependence was significant. Werner et al. then evaluated the two reported correlations for an extensive group of dinuclear Fe^{III} complexes with OH$^-$, RO$^-$, and/or phenoxide bridges (i.e., instead of O^{2-}).[21c] They concluded that the WG equation was inappropriate, i.e., that the angular dependence is insignificant

Table 3. Complexes Used in the Development of the MSC

compound[a]	J_{ij}	J_{exp}[b] (cm^{-1})	Fe–O (av) (r, Å)	Fe–O–Fe (ϕ, deg)	J_{pred}[c] (cm^{-1})	ref
$[Fe_3O(O_2C^tBu)_2(N_3)_3(dmem)_2]$	J_{12}	−3.6	2.004	96.77	−5.4	47
	J_{23}	−3.6	2.004	96.07	−5.1	
	J_{13}	−45.9	1.868	162.82	−44.3	
$[Fe_3O(Etsao)\ (benz)_5(MeOH)_2]$	J_{13}	−38	1.887	120.65	−34.9	48
	J_{23}	−38	1.906	116.44	−27.6	
	J_{12}	−29.3	1.905	122.65	−30.3	
$[Fe_3(O_2CMe)_3(L^1)_3]$	J_{12}	−10.4	2.003	120.2	−12.2	49
	J_{13}	−9.4	2.017	116.1	−10.1	
	J_{23}	−8.6	1.984	124.7	−15.2	
$[Fe_4(N_3)_6(hmp)_6]$	J_{12}	−9.2	2.031	102.6	−6.0	27a
	$J_{11'}$	−12.5	1.993	105.2	−9.4	
$[Fe_4(OMe)_2(O_2CMe)_2(L^2)_4]$	$J_{12'}$	−10.2	1.984	126.49	−15.4	49
	J_{12}	−9.2	2.020	100.75	−6.0	
$[Fe_4O_2(O_2CPh)_7(phen)_2]^+$	J_{wb}	−38.8	1.87	129.18	−43.8	50
$[Fe_4O_2(O_2C^tBu)_8(bpm)]$	J_{wb}	−36.1	1.89	122.90	−34.8	51

[a]dmem = 2-([2-(dimethylamino)ethyl]-methylamino)ethanol; Etsao = 2-hydroxy-propiophenone oxime; L^1 = fully deprotonated salicylidene-2-ethanolamine; hmp = anion of 2-(hydroxymethyl)pyridine; L^2 = fully deprotonated derivative of salicylidene-2-ethanolamine; phen = 1,10-phenanthroline; bpm = 2,2-bipyrimidine. [b]Experimental J values have been converted to the $\mathcal{H} = -2J\hat{S}_i\cdot\hat{S}_j$ convention, if necessary. [c]Predicted J values are in the $\mathcal{H} = -2J\hat{S}_i\cdot\hat{S}_j$ convention and have an error of ±3%.

and that a modified GL correlation was the best. Finally, other correlations on Fe(OR)$_2$Fe complexes have shown that J has a linear dependence on the Fe–O–Fe bridging angle.[22] *The contrasting results from these studies show that even for just dinuclear complexes, no coherent MSC emerges that is applicable to multiple types of bridging oxo ligands.* Of course, in most cases the J value can be reliably determined experimentally for such simple systems, and the correlation is primarily to rationalize the observed J, except perhaps in poorly characterized biological Fe$^{III}_2$ sites, where it can be used to deduce structural information.

Higher-Nuclearity Complexes. In our own work, we are primarily interested in higher-nuclearity Fe^{III} compounds, and we have found the previous correlations developed for dinuclear complexes to be of little use for these (vide infra). Thus, when a few years ago we were studying some Fe$_6$ clusters, we obtained estimates of the constituent J values from ZILSH theoretical calculations, adjusted somewhat by fits to the experimental $\chi_M T$ vs T data using a genetic algorithm approach, and then used them to derive a MSC appropriate for these Fe$_6$ clusters by adjusting the coefficients in the WG eq 6.[9] The new coefficients ($A = 2 \times 10^7$ cm^{-1}, $B = 0.2$, $C = -1$, and $D = -7$ Å^{-1}) differed markedly, particularly A and B, which were an order of magnitude different from the WG coefficients and pointed out to us a much different radial dependence than in dinuclear compounds. However, this correlation was focused specifically on this Fe$_6$ cluster type, and while it provided us with an improvement over the dinuclear correlations, it was not clear how reliable the ZILSH J values were on which it was based, to what extent therefore the adjusted A, B, C, D and resulting J values corresponded to the true ones (i.e., reality), and to what extent the derived correlation was applicable to other high-nuclearity structural types. Thus, prompted by several new Fe$^{III}_x$ clusters we have recently prepared, the ground states of which we could not rationalize, we decided to explore the development of a reliable MSC generally applicable to high-nuclearity Fe^{III}/oxo clusters.

Semiempirical Magnetostructural Correlation for Fe$^{III}_x$ Clusters. We used the WG format of eq 6, because of its sound grounding in the AOM, but refined its coefficients using literature oxo-bridged Fe$^{III}_n$ ($n \geq 3$) complexes to target a MSC tailored for higher-nuclearity complexes. We chose complexes for which (i) high-quality crystal structures were available; (ii) reliable J_{ij} values had been experimentally determined, specifically by fits of data collected down to 5 K in dc fields below 0.5 T; and (iii) the structures spanned various Fe$_n$ topologies in order to avoid overwhelming the model with one structural type. We found only a surprisingly limited number of complexes that satisfied all our criteria, and these are listed in Table 3. For the $[Fe_4O_2]^{8+}$ butterfly complexes, the body–body (J_{bb}) interaction was excluded because of the well-documented spin frustration that occurs along this pathway, making it difficult to experimentally determine a reliable J value.[12a] As for the previous correlations, we assumed that couplings were dominated by the pathways involving monatomic oxo bridges and that contributions through multiatomic bridges (e.g., carboxylates) were minor.

With suitable test complexes selected, a nonlinear regression was run on eq 6 using for each Fe···Fe pair the average Fe–O distance (r) and Fe–O–Fe angle (ϕ) as the independent variables and the experimentally determined J_{ij} (converted to the $\mathcal{H} = -2J\hat{S}_i\cdot\hat{S}_j$ convention, if necessary) as the dependent variable, to determine new parameters (A, B, C, and D) that best fit the data. The obtained values are shown, and thus eq 7 is the new MSC.

$$A = 1.23 \times 10^9\ \text{cm}^{-1} \quad B = -0.12 \quad C = 1.57 \quad D = -8.99\ \text{Å}^{-1}$$

$$J = (1.23 \times 10^9)(-0.12 + 1.57 \cos \phi + \cos^2 \phi) \exp(-8.99r) \qquad (7)$$

We checked it initially with the independent variables of average Fe–O distance and Fe–O–Fe angle to back-calculate the predicted J value (J_{pred}; $\mathcal{H} = -2J\hat{S}_i\cdot\hat{S}_j$ convention) for each Fe$_2$ exchange coupling in the test complexes. The very good agreement between J_{pred} and experimental (J_{exp}) values (Table 3) is also reflected in the J_{pred} vs J_{exp} scatter plot in Figure 4, which has a satisfying $R^2 = 0.93$. During these checks, we found that if an Fe$_2$ pair had more than one monatomic oxo

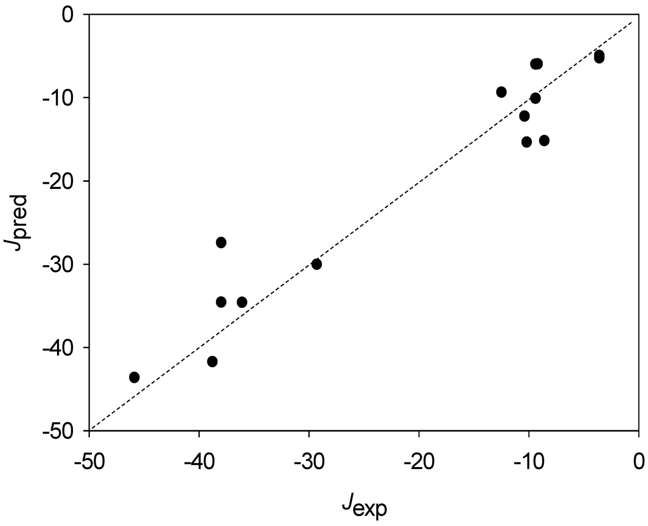

Figure 4. Scatter plot of MSC J_{pred} vs J_{exp} with R^2 = 0.93. The dashed line is the J_{pred} = $J_{exp.}$ line.

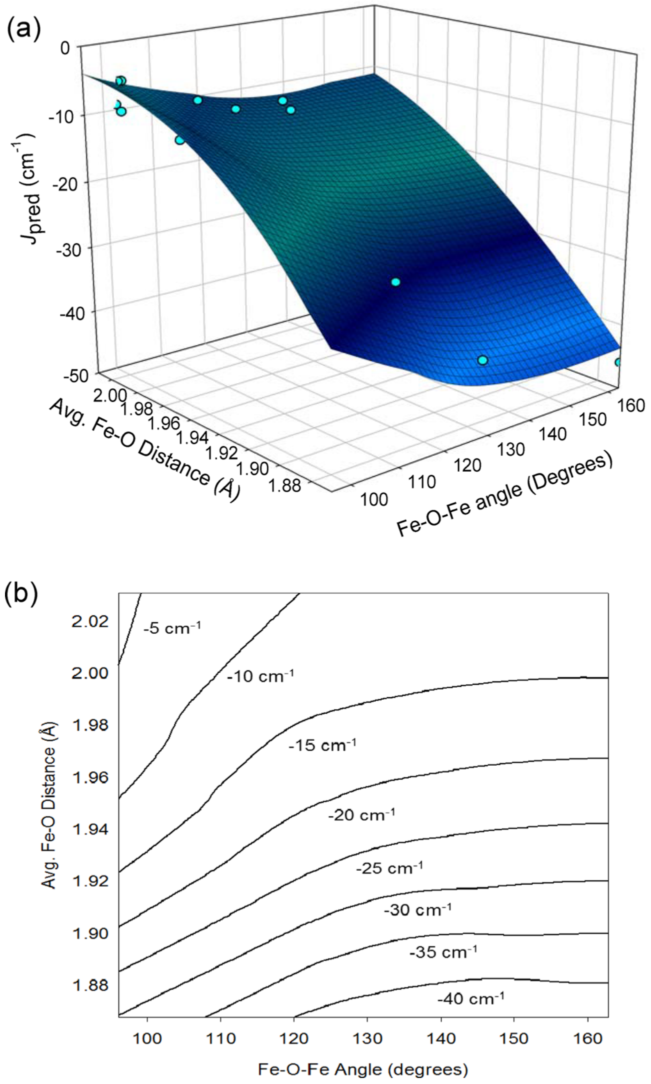

Figure 5. (a) 3D surface defined by the MSC showing the dependence of J_{pred} on average Fe–O distance and Fe–O–Fe angle. Light blue dots represent the J_{exp} for the test complexes. (b) 2D contour plot of the 3D surface emphasizing the relative dependence of J_{pred} on average Fe–O distance and Fe–O–Fe angle. Solid lines represent iso-J lines (lines of constant J).

bridge, the Fe–O–Fe pathway with the longer average Fe–O distance yielded the closer agreement with J_{exp}. An alternative depiction of the MSC of eq 7 is as a 3D surface of J_{pred} vs the average Fe–O distance and Fe–O–Fe angle (Figure 5a), where the J_{exp} values for the test complexes are included as blue points. This 3D surface allows the relative importance of the Fe–O radial and Fe–O–Fe angular dependence of J_{pred} to be evaluated, and there is clearly a significant angular dependence, even though the radial dependence is dominant. This is better seen in the 2D contour plot (Figure 5b), where iso-J lines (lines of constant J value) are far from parallel to the x-axis (Fe–O–Fe); i.e., there is a significant angular dependence, except at larger angles, where J approaches being angle-independent. In general, the exchange coupling becomes more strongly AF with decreasing Fe–O distance and increasing Fe–O–Fe angle, consistent with greater net overlap between Fe d-orbitals through the p-orbitals of the bridging O atom. Thus, J is weakest at the longest Fe–O distances and smaller Fe–O–Fe angles. Since a major difference between dinuclear and polynuclear clusters is that one or more μ_3-O^{2-} ions will usually be present in the latter, we did consider if an additional parameter might be important to the MSC, such as the distance (d) of the μ_3-O^{2-} above its Fe_3 plane, but including this as an additional term in eq 7 led to no significant improvement in the J_{pred} vs J_{exp} agreements of Table 3 and Figure 4. Therefore, for simplicity, we did not consider d any further.

Having developed the MSC for higher-nuclearity complexes, we also checked how well it might apply to μ-O^{2-}-bridged dinuclear compounds, specifically the 32 used to develop the WG equation.[21b] As expected, we obtained a very poor correlation between J_{pred} and J_{exp} (R^2 = 0.21), which is consistent with our previous conclusion that the GL and WG correlations are of little use for higher-nuclearity clusters.

Application of the New MSC: Rationalization of Spin Ground States. The MSC was now applied to the new complexes **1** (Fe_8) and **2** (Fe_6) from this work and previously reported $[Fe_5O_2(OH)(O_2CMe)_5(hmbp)_3](ClO_4)_2$ (**3**),[37] to assess its ability to predict the constituent exchange couplings and rationalize the experimentally determined ground states of S = 0, 5, and $^5/_2$, respectively, by identifying the relative spin alignments at the metal ions and any spin-frustrated pathways. The results are shown in Figure 6. For **1** (Figure 6a, Table 4), the obtained J_{pred} separate into two groups, strong ($|J_{pred}| > 27\ cm^{-1}$) and weak ($|J_{pred}| < 10\ cm^{-1}$), corresponding to Fe_2 pairs with one and two monatomic oxo bridges, respectively. As a result, each triangular Fe_3 subunit within **1** has two strong and one weak J_{pred}. An AF M_3 triangle is the textbook example of a spin-frustrated system, but with one weak and two strong competing AF interactions, the weak ones will be completely frustrated (J_{12}, J_{34}, and $J_{11'}$ shown in red) and the spin alignments will be determined by the strong couplings, giving a classical "spin up, spin down" pattern corresponding to $m_S = \pm ^5/_2$ z-components of spin. The predicted alignments are thus as shown in Figure 6a, with spins coupled by the weak J_{pred} forced parallel by the strong couplings, giving a total spin of S = 10–10 = 0, in agreement with the experimental data. Of course, because the ground state is a singlet, the local z-components of spin at each metal are actually zero because the wave function is a linear combination of a number of equally weighted pairs of components with reversed z-components of spin. The primary components of the wave function in this case will be the one shown in Figure 6a and the one with all spin alignments reversed. We also include for

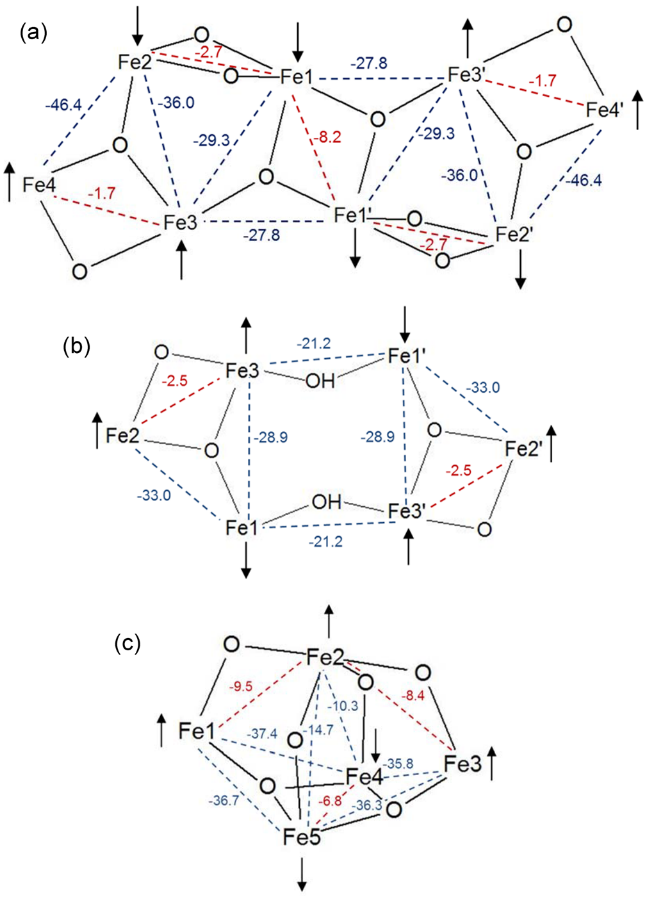

Figure 6. Core of complexes **1** (a), **2** (b), and **3** (c) showing MSC J_{pred} values (cm^{-1}) calculated using the MSC (eq 7), and the predicted spin alignments rationalizing the $S = 0$, 5, and $^5/_2$ ground states, respectively; frustrated interactions are shown in red.

Table 4. Predicted J_{ij} Values[a] for 1 from various MSC's

J_{ij}	J_{GL}[b]	J_{WG}[c]	J_{Werner}[d]	J_{pred}[e]
$J_{11'}$	−18.7	−46.5	−18.6	−8.2
J_{12}	−9.1	−28.0	−12.7	−2.7
J_{13}	−29.3	−48.9	−23.7	−29.3
J_{23}	−33.6	−48.0	−25.5	−36.0
J_{24}	−54.6	−71.2	−33.1	−46.4
$J_{13'}$	−23.7	−39.0	−21.1	−27.8
J_{34}	−28.8	−56.0	−23.5	−1.7

[a] In cm^{-1}; converted to the $\mathcal{H} = -2J\hat{S}_i\cdot\hat{S}_j$ convention, if necessary [b] Reference 21a. [c] Reference 21b. [d] Reference 21c. [e] New MSC of eq 7.

comparison in Table 4 the values calculated using the previous MSC's developed for dinuclear complexes: Their J_{pred} are of more comparable magnitudes and would thus predict several intermediate spin alignments; even if they then predicted the correct ground state, it would be fortuitous. It is particularly interesting that one of the weaknesses of the previous MSC's is their inability to correctly identify weak couplings arising from bis-oxo-bridged Fe_2 pairs ($J_{11'}$, J_{12}, J_{34}), these being correctly predicted by the new MSC (and confirmed by DFT calculations of such pairs in, for example, Fe_4[35a] and Fe_7[38] clusters).

We can similarly rationalize the ground states of **2** and **3**. For **2**, the calculated J_{pred} from the MSC (Figure 6b) are again relatively strong ($|J_{pred}| > 20\ cm^{-1}$) and weak ($J_{pred} = -2.5\ cm^{-1}$) due to one and two oxo bridges, respectively (Table 5). This should lead to complete frustration of the weak interactions and the resulting alignments shown in Figure 6b, giving an $S = 10-5 = 5$ ground state. For **3**, relatively strong ($|J_{pred}| > 35\ cm^{-1}$) and weak ($|J_{pred}| < 10\ cm^{-1}$) interactions are calculated (Figure 6c, Table 6), the former all within the butterfly unit (Fe1, Fe3, Fe4, Fe5). These four spins will therefore be aligned antiparallel to their neighbors on the outside ("body–wingtip") edges of the butterfly, frustrating the inner ("body–body") J_{45} interaction and giving an $S_b = 0$ ground state for the butterfly unit. The $S = {}^5/_2$ ground state for the whole molecule can then be rationalized as simply arising from the spin of apical Fe2. We show it aligned vertically on the basis of the J values to the other Fe atoms, but it is best to think of the $S = {}^5/_2$ ground state as arising from the spin of Fe2 plus a diamagnetic Fe_4 butterfly unit. In fact, this description was what was originally hypothesized for **3**[37] on the basis of the known $S = 0$ ground states of Fe^{III}_4 butterfly clusters, and it is now supported by the more quantitative considerations of the present work.

Analysis of the Fe_8 Single-Molecule Magnet with $S = 10$. One of the first and most-well-studied SMMs is the $[Fe_8O_2(OH)_{12}(tacn)_6]^{8+}$ (**4**; Figure 7) cation, which possesses an $S = 10$ ground state due to spin frustration from competing interactions. The exchange interactions have previously been investigated both experimentally and theoretically, allowing for a useful comparison of previous results with the J_{pred} from the new MSC. These data are collected in Table 7. There is very good agreement between the J_{pred} values and those from the ZILSH calculation,[39] both of which employ the crystallographic C_1 symmetry. The biggest disagreements are for the strongly AF interactions within subgroup J_C, which all the studies conclude are the strongest in the complex. The DFT calculations using the PBE and B3LYP functionals[40] give overall good agreement with the MSC J_{pred} (particularly B3LYP), but the ferromagnetic (F) values for the J_{18} (J_{bb}) interaction are unrealistic for oxo-bridged high-spin Fe^{III}, as discussed in detail elsewhere.[39] The experimental J_{exp} values, obtained from simulations of experimental $\chi_M T$ vs T data,[41] are in fair agreement with the DFT/ZILSH and MSC J_{pred} for the J_A and J_B interactions, but they give J_C values that are far too strong by a factor of 2; values of $-70\ cm^{-1}$ are simply unrealistic for an Fe_2 pair in a cluster bridged by a μ_3-O^{2-} ion and would be more consistent with the shorter Fe–O bonds in a dinuclear Fe^{III}_2 complex bridged by a single μ-O^{2-} ion, as seen in the GL and WG studies.

All the studies in Table 7 predict an $S = 10$ ground state for **4**, because they all conclude that the eight strong AF J_B and J_C interactions dominate and determine the spin alignments, as shown in Figure 7 with the new J_{pred} values. As observed for **1** and **2**, each Fe_3 triangle within **4** has two strong and one weak AF interactions, the latter are completely frustrated, and the spin alignments are thus again in a classical spin-up/spin-down pattern to give an $S = 15-5 = 10$ ground state. Nevertheless, we feel that the new MSC has yielded the most reliable values to date across all four sets of exchange interactions in **4**, with no unreasonable values in terms of magnitude or sign.

Fitting of Magnetic Susceptibility Data. As stated earlier, an important application of a reliable MSC is to obtain reasonable approximations of the J values of higher-nuclearity clusters for use as starting points in fits of magnetic data, with the hope that this will lead to the true J values for the compound instead of those at a local fit minimum. We have therefore employed the predictive capability of the MSC to assist fits of VT magnetic susceptibility

Table 5. J_{ij} Values[a] for 2 from Fits Using Different Initial J_{ij} Values

J_{ij}[b]	J_{pred}	Fit_{MSC}[c]	$Fit_{MSC}(C_1)$[d]	$Fit_{(0)}$[e]	$Fit_{(-10)}$[e]	$Fit_{(-20)}$[e]	$Fit_{(-30)}$[e]
J_{12}	−33.0	−28.2	−27.1	+19.4	−32.6	−26.9	−28.7
J_{13}	−28.9	−28.5	−31.3	−71.2	−13.8	−36.8	−34.6
J_{23}	−2.5	−3.2	−3.1	−58.5	−2.1	−1.6	−1.6
$J_{13'}$	−21.2	−17.7	−19.1	−6.8	−27.6	−12.8	−11.5
$J'_{1'2'}$			−29.6				
$J'_{1'3'}$			−25.9				
$J'_{2'3'}$			−3.3				
$J'_{1'3}$			−16.4				
TIP[f]		600	600	600	600	600	600
zJ[g]		−0.005	−0.005	−0.005	−0.005	−0.005	−0.005

[a] In cm^{-1} [b] J and J' are related by the crystallographic inversion center. [c] Fit values using the MSC J_{pred} as input J_{ij} values. [d] Fit values using the MSC J_{pred} as input, and all J_{ij} independent. [e] $Fit_{(n)}$ data are fit values using input J_{ij} of n cm^{-1}. [f] Temperature-independent paramagnetism, $\times 10^{-6}$ cm^3 mol^{-1}. [g] Mean-field correction.

Table 6. J_{ij} Values[a] for 3 from Fits Using Different Initial J_{ij} Values

J_{ij}	J_{pred}	Fit_{MSC}[b]	$Fit_{MSC}(C_{2v})$[c]	$Fit_{(0)}(C_{2v})$[d]	$Fit_{(-10)}(C_{2v})$[d]	$Fit_{(-20)}(C_{2v})$[d]	$Fit_{(-30)}(C_{2v})$[d]
J_{12}	−9.5	−11.6	−7.3	−30.1	+172.2	−36.7	−33.7
J_{23}	−8.4	−2.1	−7.3	−30.1	+172.2	−36.7	−33.7
J_{14}	−37.4	−36.6	−30.6	−22.1	−39.5	−10.1	−11.3
J_{15}	−36.7	−36.6	−30.6	−22.1	−39.5	−10.1	−11.3
J_{24}	−10.3	−13.8	−8.0	−52.5	−46.3	−13.4	−16.0
J_{25}	−14.7	+5.0	−8.0	−52.5	−46.3	−13.4	−16.0
J_{34}	−35.8	−24.4	−30.6	−22.1	−39.5	−10.1	−11.3
J_{35}	−36.3	−35.7	−30.6	−22.1	−39.5	−10.1	−11.3
J_{45}	−6.8	−12.2	−9.6	+37.0	−38.3	−32.6	−33.1
TIP[e]		500	500	500	500	500	500
zJ[f]		−0.021	−0.021	−0.021	−0.021	−0.021	−0.021

[a] In cm^{-1} [b] Fit values using the MSC J_{pred} as input J_{ij} values. [c] Fit values using the MSC J_{pred} as input J_{ij} values and imposing virtual C_{2v} symmetry. [d] $Fit_{(n)}$ data are fit values using input J_{ij} of n cm^{-1}. [e] Temperature-independent paramagnetism, $\times 10^{-6}$ cm^3 mol^{-1}. [f] Mean-field correction.

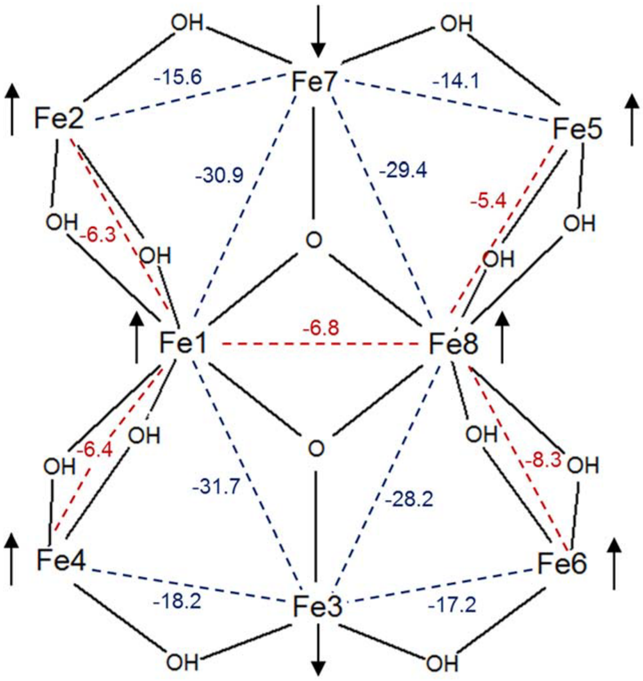

Figure 7. Core of complex **4** showing MSC J_{pred} values (cm^{-1}) and the predicted spin alignments rationalizing the $S = 10$ ground state; frustrated pathways are shown in red.

data using the program PHI.[42] We chose **2** and **3** as two reasonably complicated test clusters for this investigation.

Table 7. Comparison of Exchange Interactions (cm^{-1}) Otained for 4 from Theoretical Calculations, Experimental Data, and the MSC

pathway[a]		J_{PBE}	J_{B3LYP}	J_{ZILSH}	J_{exp}[b]	J_{pred}[c]
J_{bb}	J_{18}	+14.5	+2.6	−4.7	−12.5	−6.8
J_A	J_{12}	−4.6	−5.2	−8.8	−9.0	−6.3
	J_{14}			−9.7		−6.4
	J_{58}			−8.4		−5.4
	J_{68}			−9.0		−8.3
J_B	J_{27}	−7.2	−17.1	−16.6	−20.5	−15.6
	J_{34}			−18.2		−18.2
	J_{36}			−17.0		−17.2
	J_{57}			−15.3		−14.1
J_C	J_{17}	−27.9	−33.3	−44.5	−70.0	−30.9
	J_{13}			−47.4		−31.7
	J_{38}			−43.9		−28.2
	J_{78}			−44.2		−29.4

[a] Adapted from the table reported by O'Brien and O'Callaghan. The subgroups J_{bb}, J_A, J_B, and J_C result from imposing the virtual D_2 symmetry of the molecule. [b] From a simulation of the experimental $\chi_M T$ vs T data; converted to the $\mathcal{H} = -2J\hat{S}_i \cdot \hat{S}_j$ convention.[41] [c] From the new MSC of eq 7.

The first step was to assess how closely the VT dc $\chi_M T$ vs T plots for **2** and **3**, calculated by PHI using the MSC J_{pred} values, compare with the experimental data. The obtained plots [Figure 8, purple (**2**) and green (**3**) lines] are overall satisfyingly similar to the experimental data, in both profile and predicted ground state, for such complicated molecules with

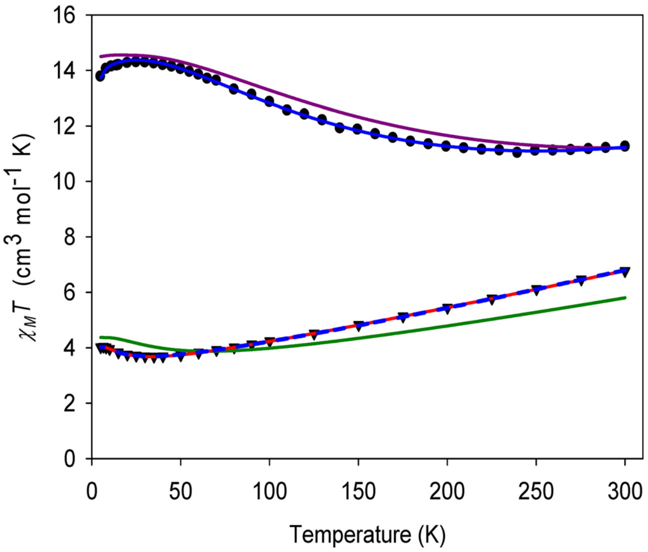

Figure 8. Experimental $\chi_M T$ vs T data for $\mathbf{2}\cdot 4H_2O$ (●) and **3** (▼), simulated $\chi_M T$ vs T using the MSC J_{pred} for $\mathbf{2}\cdot 4H_2O$ (purple line) and **3** (green line), and fits of experimental $\chi_M T$ vs T data using J_{pred} inputs for $\mathbf{2}\cdot 4H_2O$ (blue line), **3** (red line), and **3** with imposed C_{2v} symmetry (dashed blue line).

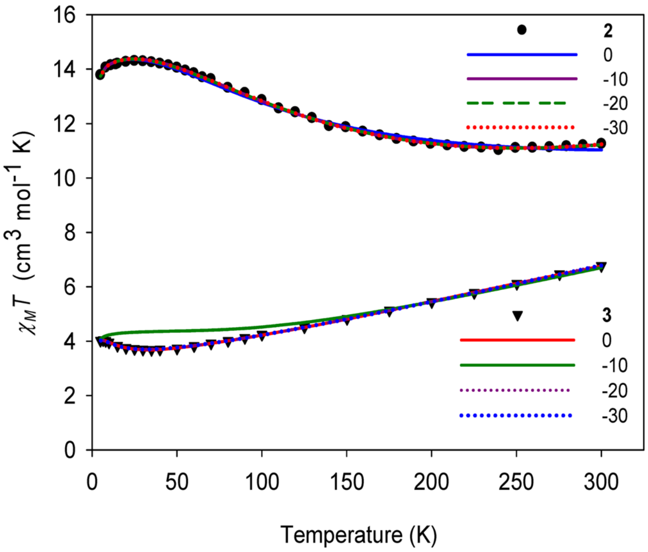

Figure 9. Experimental $\chi_M T$ vs T for $\mathbf{2}\cdot 4H_2O$ (●) and **3** (▼) and the four fits with the indicated input values (cm^{-1}) for all J_{ij}.

multiple independent interactions. To improve the agreement further, the data were fit using the J_{pred} as inputs (starting values); PHI requires input values for each J_{ij} parameter. For centrosymmetric **2**, four J_{pred} were input and an excellent fit was obtained (Figure 8, blue line) with J_{ij} (Fit$_{MSC}$) values only slightly different from the J_{pred} inputs (Table 5). If symmetry-related J_{ij} (J and J' in Table 5) are allowed to vary independently, the fit using J_{pred} inputs, Fit$_{MSC}$(C_1), gives values similar to Fit$_{MSC}$, with the most different pairs (J_{13} vs $J'_{1'3'}$ and $J_{13'}$ vs $J'_{1'3}$) giving averages essentially identical to the Fit$_{MSC}$ values. For **3**, the crystallographic C_1 symmetry required nine input J_{pred} and the obtained fit (Fit$_{MSC}$) was excellent (Figure 8, red line), but the fit values (Table 6, Fit$_{MSC}$) were in some cases either ferromagnetic (J_{25}) and/or unreasonably different for J_{ij} pairs related by virtual symmetry [and thus with similar Fe−O and Fe−O−Fe structural parameters (e.g., J_{12}/J_{23} and J_{34}/J_{35}) and resulting J_{pred}]. In this case, it was clear that the virtual C_{2v} symmetry should be imposed, both to prevent overparameterization and to ensure that structurally equivalent Fe_2 pairs have the same J_{ij}. The resulting fit was excellent (Figure 8, dashed blue line) and gave values reasonably similar to J_{pred}.

Of course, it could be argued that PHI could have given excellent fits directly, with J_{ij} values similar to those in Tables 5 and 6, without the extra step of first calculating MSC J_{pred} as inputs. We thus explored fits with arbitrary J_{ij} inputs of 0, −10, −20, and −30 cm^{-1}. For both **2** and **3** (C_{2v}), the fits were all excellent except for Fit$_{(-10)}$ for **3** (Figure 9), but the fit J_{ij} values varied remarkably with input in both magnitude and sign (Tables 5 and 6). For Fit$_{(-10)}$ for **3**, the program reproducibly followed paths that led to poorer local minima; no doubt we could have adjusted something to also get excellent fits with these inputs, but for consistency and since our primary interest was in comparing the fits under identical conditions, we did not explore this. If the centrosymmetry is removed, the results for **3** are even worse (Table S3, SI).

The conclusion we reach from these studies is that excellent fits can be obtained for both **2** and **3**, the J_{ij} parameters of which are nevertheless grossly unacceptable, with little resemblance to expected reality in both sign and/or magnitude; ferromagnetic J_{ij}, for example, are simply unreasonable for oxo-bridged high-spin Fe^{III}. Even with only four J_{ij} parameters in each case, there are clearly many local error minima and the obtained fit values are thus very sensitive to inputs. The latter is a well-recognized problem in multiparameter fits, of course, but we were nevertheless surprised at the dramatic variations we encountered. Indeed, this supports the validity and importance of one of our main objectives, to develop a MSC giving reliable J_{pred} so that subsequent fits can, with some confidence, be taken as reasonably reflecting the "true" J_{ij} for higher-nuclearity clusters.

Temperature-independent paramagnetism (TIP) and intermolecular interactions (zJ) will also contribute to the experimental data and were included in our study. These are given in Tables 5 and 6, and their values were decided upon in the following manner. For TIP, we determined that a value of 100×10^{-6} per Fe ion yielded the best results after investigating the fits with added TIP of 0, 100, and 200 ($\times 10^{-6}$) cm^3 mol^{-1} per Fe (Tables S4 and S5, SI). In fact, as long as some TIP was included, the fits were not particularly sensitive to the exact amount. The zJ term will be most important at the lowest T and was determined by manually adjusting its value to best fit these lowest T data.

Protocol for Application of the MSC. From the above results, we can formulate a protocol for applying the new MSC to high-nuclearity Fe^{III}/oxo clusters:

(a) Using the averaged Fe−O bond distance and Fe−O−Fe angle, determine the J_{pred} for each Fe_2 pair in the molecule using eq 7. If there are two monatomic Fe−O−Fe pathways for a given Fe_2 pair, the longer average Fe−O distance should be employed; this yields the best results vis-à-vis experimental data, since these pathways will have weak interactions.

(b) For most clusters, the relative magnitudes of the obtained MSC J_{pred} will be sufficient to rationalize the experimental ground state S from the predicted spin alignments at each Fe^{III}, even when there are competing J_{pred} interactions within triangular Fe_3 subunits.

(c) If desired, the MSC J_{pred} can be used to simulate the dc $\chi_M T$ vs T plots, using a program such as PHI or a similar one, for comparison with the experimental plots.

DOI: 10.1021/acs.inorgchem.6b00769
Inorg. Chem. 2016, 55, 6597−6608

(d) The MSC J_{pred} can then be refined by fitting the experimental dc $\chi_M T$ vs T data using the J_{pred} as input values. The virtual symmetry of the molecule should be imposed to avoid overparameterization.

■ CONCLUSIONS

The use of hqnH and benzoic acid in Fe^{III} chemistry has yielded two polynuclear clusters **1** and **2** that show some structural differences with those previously obtained with hmpH, assignable to the less flexible nature of hqn^-. **1** and **2** possess $S = 0$ and $S = 5$ ground states, respectively, which can be qualitatively assigned to the presence of spin frustration within the triangular Fe_3 subunits with all-AF interactions.

In order to more quantitatively rationalize the experimentally observed ground states of **1** and **2**, and other Fe^{III}_x/O ($x \geq 4$) clusters, we have derived a semiempirical MSC for Fe^{III}/O clusters using reliable crystal structure and experimental magnetic susceptibility data in the literature. The new MSC uses only the observed Fe−O bond lengths and Fe−O−Fe angles and has yielded J_{pred} values that have proven satisfyingly successful in explaining the experimentally derived ground states of several Fe_x clusters. Further, we have found that the J_{pred} values represent excellent starting points for fits of dc $\chi_M T$ vs T data, giving physically reasonable fit parameters that can be taken with some confidence as reflecting the true exchange parameters (i.e., reality), as long as some straightforward measures are taken to avoid certain problems identified during our control studies. The obtained results have been amalgamated into a protocol that is described for the use of the new MSC. Although the new MSC is specifically for Fe^{III}/O clusters, these are extremely common in the literature due to the importance of this chemistry in a number of disparate fields. In addition, it covers all types of monatomic bridging oxo groups, i.e., O^{2-}, OH^-, OR^-, etc., and thus is distinctly different from the dinuclear MSCs available to date.

■ EXPERIMENTAL SECTION

All manipulations were performed under aerobic conditions using chemicals and solvents as received, unless otherwise stated. $[Fe_3O(O_2CPh)_6(H_2O)_3](NO_3)$ was prepared as reported previously.[9] hqnH is 8-hydroxyquinoline.

Synthesis of $[Fe_8O_4(OMe)_2(O_2CPh)_{10}(hqn)_4]$ (1). *Method A.* To a stirred solution of $PhCO_2H$ (0.24 g, 4.0 mmol) were added hqnH (0.076 g, 1.0 mmol) and NEt_3 (0.42 mL, 6.0 mmol), followed by $Fe(NO_3)_3 \cdot 9H_2O$ (0.40 g, 2.0 mmol), which caused the solution to turn essentially black and begin depositing a gray precipitate. The slurry was stirred a further 30 min and then filtered, and the gray precipitate was washed with MeOH and allowed to dry. The powder was dissolved in CH_2Cl_2, layered with hexanes, and left undisturbed for 4 days at room temperature, during which time black plates of $\mathbf{1} \cdot 4CH_2Cl_2$ slowly formed. Crystals for X-ray crystallographic studies were maintained in mother liquor; otherwise, they were collected by filtration, washed with hexanes, and dried under vacuum for other studies. The yield was 26% based on Fe. Anal. Calcd (Found) for $\mathbf{1} \cdot 3H_2O$ ($C_{108}H_{86}Fe_8N_4O_{33}$): C, 53.72 (53.83); H, 3.59 (3.34); N, 2.32 (2.13). Selected IR data (KBr disk, cm^{-1}): 3446 (mb), 3062 (w), 2918 (w), 2807 (w), 1599 (s), 1556 (s), 1497 (s), 1467 (s), 1411 (s), 1321 (m), 1275 (w), 1175 (w), 1110 (m), 1067 (w), 1026 (w), 824 (w), 786 (w), 717 (s), 674 (m), 642 (w), 617 (w), 592 (m), 521 (m), 473 (m).

Method B. To a stirred solution of $[Fe_3O(O_2CPh)_6(H_2O)_3](NO_3)$ (0.25 g, 0.25 mmol) in MeOH (20 mL) was added hqnH (0.036 g, 0.25 mmol), which caused the solution to change from bright orange to black. NEt_3 (0.14 mL, 1.0 mmol) was added and the solution stirred for a further 30 min, during which time a gray precipitate formed. The solution was filtered and the precipitate was washed with MeOH and allowed to dry. The powder was then recrystallized as in method A. The yield was 11% based on Fe. The identity of the product was confirmed by IR spectral and unit cell comparisons with material from method A.

$[Fe_6O_2(OH)_2(O_2CPh)_{10}(hqn)_2]$ (2). To a stirred orange suspension of $[Fe_3O(O_2CPh)_6(H_2O)_3](NO_3)$ (0.25 g, 0.25 mmol) in H_2O (20 mL) was added hqnH (0.036 g, 0.25 mmol). The solids slowly dissolved, and the solution was stirred for ~3 h, during which time it slowly darkened and deposited a gray precipitate. The gray powder was collected by filtration, washed copiously with H_2O, and allowed to dry. It was then dissolved in CH_2Cl_2, layered with hexanes, and left undisturbed for 4 days at room temperature, during which time black plates of $\mathbf{2} \cdot CH_2Cl_2$ slowly formed. Crystals for X-ray crystallographic studies were maintained in mother liquor; otherwise, they were collected by filtration, washed with hexanes, and dried under vacuum for other studies. The yield was 30% based on Fe. Anal. Calcd (Found) for $\mathbf{2} \cdot 4H_2O$ ($C_{88}H_{72}Fe_6N_2O_{30}$): C, 53.58 (53.73); H, 3.68 (3.81); N, 1.42 (1.72). Selected IR data (KBr disk, cm^{-1}): 3440 (b), 3061 (w), 1600 (m), 1539 (s), 1498 (s), 1469 (s), 1410 (s), 1322 (m), 1175 (w), 1112 (w), 1103 (w), 1026 (w), 825 (w), 786 (w), 716 (s), 689 (w), 677 (w), 472 (m).

X-ray Crystallography. Data were collected for $\mathbf{1} \cdot 4CH_2Cl_2$ and $\mathbf{2} \cdot CH_2Cl_2$ at 100 K on a Bruker DUO diffractometer using Mo Kα radiation (λ = 0.710 73 Å) and an APEXII CCD area detector (see Table 8). The structure was solved and refined in SHELXTL6.1[43] for $\mathbf{1} \cdot 4CH_2Cl_2$ and SHELXTL2014[44] for $\mathbf{2} \cdot CH_2Cl_2$, using full-matrix least-squares refinement on F^2. The non-H atoms were refined with anisotropic thermal parameters and all C-bound H atoms were placed in calculated, idealized positions and refined as riding on their parent C atoms.

Table 8. Crystal Data and Structure Refinement Parameters for 1 and 2

	$\mathbf{1} \cdot 4CH_2Cl_2$	$\mathbf{2} \cdot 2CH_2Cl_2$
formula[a]	$C_{112}H_{88}Cl_8Fe_8N_4O_{30}$	$C_{90}H_{64}Cl_4Fe_6N_2O_{26.15}$
fw, g mol^{-1}	2700.26	2068.73
space group	$P2_1/n$	*Pbca*
a, Å	18.2729(11)	21.6936(13)
b, Å	16.5506(10)	17.4045(10)
c, Å	19.4689(12)	23.6770(14)
α, deg	90	90
β, deg	110.037(1)	90
γ, deg	90	90
V, $Å^3$	5531.5(6)	8939.6(9)
Z	2	4
T, K	100(2)	100(2)
λ, Å[b]	0.71073	0.71073
ρ_{calc}, g cm^{-3}	1.621	1.537
μ, mm^{-1}	1.292	1.146
R_1[c,d]	0.0441	0.0336
wR_2[e]	0.1120	0.0685

[a]Including solvent molecules. [b]Graphite monochromator. [c]$I > 2\sigma(I)$. [d]$R_1 = 100\sum(||F_o| - |F_c||)/\sum|F_o|$. [e]$wR_2 = 100[\sum[w(F_o^2 - F_c^2)^2]/\sum[w(F_0^2)^2]]^{1/2}$, $w = 1/[\sum^2(F_o^2) + [(ap)^2 + bp]$, where $p = [\max(F_o^2,0) + 2F_c^2]/3$.

For $\mathbf{1} \cdot 4CH_2Cl_2$, the asymmetric unit consists of a half-Fe_8 cluster and two CH_2Cl_2 solvent molecules. Both of the latter are disordered: one was refined at two positions, while the other was refined at three positions. The disorders were modeled using the SADI command to keep all C−Cl distances similar during the least-squares refinement. In the final cycle of refinement, 12 718 reflections [of which 8655 were observed with $I > 2\sigma(I)$] were used to refine 773 parameters, and the resulting R_1, wR_2, and GOF (goodness of fit) were 4.41%, 11.20%, and 1.022, respectively.

For $\mathbf{2} \cdot CH_2Cl_2$, the asymmetric unit consists of a half-Fe_6 cluster and one disordered CH_2Cl_2 molecule. The H atom (H2) on O2 was obtained from a difference Fourier map and refined freely. Only one of the Cl atoms of the CH_2Cl_2 was disordered, and it was refined at two positions with the site occupation factors dependently refined. In the final cycle of refinement, 10 282 reflections [of which 6611 were observed with $I > 2\sigma(I)$] were used to refine 595 parameters, and the resulting R_1, wR_2, and GOF were 3.36%, 6.85%, and 0.890, respectively.

Physical Measurements. Infrared spectra were recorded in the solid state (KBr pellets) on a Nicolet Nexus 670 FTIR spectrometer in the 400−4000 cm^{-1} range. Elemental analyses (C, H, and N) were performed by the in-house facilities of the University of Florida, Chemistry Department, for **1** and at Complete Analysis Laboratories, Inc. for **2**. Variable-temperature direct current (dc) and alternating current (ac) magnetic susceptibility data were collected on a Quantum Design MPMS-XL SQUID magnetometer equipped with a 7 T magnet operating in the 1.8 to 300 K range. Samples were embedded in solid eicosane to prevent torquing. Magnetization vs field and temperature data were fit using the program MAGNET.[45] Pascal's constants[46] were used to estimate the diamagnetic corrections, which were subtracted from the experimental susceptibilities to give the molar paramagnetic susceptibility (χ_M).

ASSOCIATED CONTENT

Supporting Information

The Supporting Information is available free of charge on the ACS Publications website at DOI: 10.1021/acs.inorgchem.6b00769.

X-ray crystallographic files in CIF format for complex $\mathbf{1}\cdot 4CH_2Cl_2$ and $\mathbf{2}\cdot CH_2Cl_2$ (CIF)

Tables of bond valence sums for **1** and **2** and J_{ij} values for **2** and **3** and plots of in-phase and out-of-phase ac magnetic susceptibility data for $\mathbf{1}\cdot 3H_2O$ and $\mathbf{2}\cdot 4H_2O$ (Figures S1 and S2 and Tables S1−S5) (PDF)

AUTHOR INFORMATION

Corresponding Author

*E-mail: christou@chem.ufl.edu. Phone: +1-352-392-8314. Fax: +1-352-392-8757.

Notes

The authors declare no competing financial interest.

ACKNOWLEDGMENTS

We thank the National Science Foundation (Grant DMR-1213030) for support of this work.

REFERENCES

(1) (a) Arii, H.; Nagatomo, S.; Kitagawa, T.; Miwa, T.; Jitsukawa, K.; Einaga, H.; Masuda, H. *J. Inorg. Biochem.* **2000**, *82*, 153−162. (b) Mauerer, B.; Crane, J.; Schuler, J.; Wieghardt, K.; Nuber, B. *Angew. Chem., Int. Ed. Engl.* **1993**, *32*, 289−291. (c) Toftlund, H.; Murray, K. S.; Zwack, P. R.; Taylor, L. F.; Anderson, O. P. *J. Chem. Soc., Chem. Commun.* **1986**, 191−193.

(2) (a) Menage, S.; Zang, Y.; Hendrich, M. P.; Que, L. *J. Am. Chem. Soc.* **1992**, *114*, 7786−7792. (b) Herold, S.; Lippard, S. J. *J. Am. Chem. Soc.* **1997**, *119*, 145−156. (c) Lee, D.; Lippard, S. J. *J. Am. Chem. Soc.* **1998**, *120*, 12153−12154.

(3) (a) Kim, K.; Lippard, S. J. *J. Am. Chem. Soc.* **1996**, *118*, 4914−4915. (b) Coucouvanis, D.; Reynolds, R. A.; Dunham, W. R. *J. Am. Chem. Soc.* **1995**, *117*, 7570−7571. (c) Costas, M.; Rohde, J.-U.; Stubna, A.; Ho, R. Y. N.; Quaroni, L.; Münck, E.; Que, L. *J. Am. Chem. Soc.* **2001**, *123*, 12931−12932. (d) Sankaralingam, M.; Palaniandavar, M. *Polyhedron* **2014**, *67*, 171−180.

(4) (a) Kurtz, D. M., Jr. *Chem. Rev.* **1990**, *90*, 585−606. (b) Lippard, S. J. *Angew. Chem., Int. Ed. Engl.* **1988**, *27*, 344−361. (c) Tshuva, E. Y.; Lippard, S. J. *Chem. Rev.* **2004**, *104*, 987−1012.

(5) (a) Jambor, J. L.; Dutrizac, J. E. *Chem. Rev.* **1998**, *98*, 2549−2586. (b) Cornell, R. M.; Schwertmann, U. *The Iron Oxides*; Wiley-VCH Verlag GmbH & Co. KGaA, 2004. (c) Fortin, D.; Langley, S. *Earth-Sci. Rev.* **2005**, *72*, 1−19. (d) Michel, F. M.; Ehm, L.; Antao, S. M.; Lee, P. L.; Chupas, P. J.; Liu, G.; Strongin, D. R.; Schoonen, M. A. A.; Phillips, B. L.; Parise, J. B. *Science* **2007**, *316*, 1726−1729.

(6) (a) Bertini, I.; Gray, H. B.; Lippard, S. J.; Valentine, J. S. *Bioinorganic Chemistry*; University Science Books: Mill Valley, CA, 1994. (b) Xu, B.; Chasteen, N. D. *J. Biol. Chem.* **1991**, *266*, 19965−19970.

(7) (a) Theil, E. C. *Annu. Rev. Biochem.* **1987**, *56*, 289−315. (b) Theil, E. C.; Matzapetakis, M.; Liu, X. *JBIC, J. Biol. Inorg. Chem.* **2006**, *11*, 803. (c) Ford, G. C.; Harrison, P. M.; Rice, D. W.; Smith, J. M. A.; Treffry, A.; White, J. L.; Yariv, J. *Philos. Trans. R. Soc., B* **1984**, *304*, 551−565.

(8) (a) Foguet-Albiol, D.; Abboud, K. A.; Christou, G. *Chem. Commun.* **2005**, 4282−4284. (b) Taguchi, T.; Thompson, M. S.; Abboud, K. A.; Christou, G. *Dalton Trans.* **2010**, *39*, 9131−9139. (c) Gass, I. A.; Milios, C. J.; Evangelisti, M.; Heath, S. L.; Collison, D.; Parsons, S.; Brechin, E. K. *Polyhedron* **2007**, *26*, 1835−1837.

(9) Cañada-Vilalta, C.; O'Brien, T. A.; Brechin, E. K.; Pink, M.; Davidson, E. R.; Christou, G. *Inorg. Chem.* **2004**, *43*, 5505−5521.

(10) (a) Weighardt, K.; Pohl, K.; Jibril, I.; Huttner, G. *Angew. Chem., Int. Ed. Engl.* **1984**, *23*, 77−78. (b) Barra, A. L.; Debrunner, P.; Gatteschi, D.; Schulz, C. E.; Sessoli, R. *Europhys. Lett.* **1996**, *35*, 133−138.

(11) Powell, A. K.; Heath, S. L.; Gatteschi, D.; Pardi, L.; Sessoli, R.; Spina, G.; Del Giallo, F.; Pieralli, F. *J. Am. Chem. Soc.* **1995**, *117*, 2491−2502. (b) Mukherjee, S.; Bagai, R.; Abboud, K. A.; Christou, G. *Inorg. Chem.* **2011**, *50*, 3849−3851.

(12) (a) McCusker, J. K.; Vincent, J. B.; Schmitt, E. A.; Mino, M. L.; Shin, K.; Coggin, D. K.; Hagen, P. M.; Huffman, J. C.; Christou, G.; Hendrickson, D. N. *J. Am. Chem. Soc.* **1991**, *113*, 3012−3021. (b) Kahn, O. *Chem. Phys. Lett.* **1997**, *265*, 109−114.

(13) (a) Bagai, R.; Christou, G. *Chem. Soc. Rev.* **2009**, *38*, 1011−1026. (b) Christou, G.; Gatteschi, D.; Hendrickson, D. N.; Sessoli, R. *MRS Bull.* **2000**, *25*, 66−71. (c) Gatteschi, D.; Fittipaldi, M.; Sangregorio, C.; Sorace, L. *Angew. Chem., Int. Ed.* **2012**, *51*, 4792−4800. (d) Barra, A. L.; Caneschi, A.; Cornia, A.; Fabrizi de Biani, F.; Gatteschi, D.; Sangregorio, C.; Sessoli, R.; Sorace, L. *J. Am. Chem. Soc.* **1999**, *121*, 5302−5310.

(14) Crawford, V. H.; Richardson, H. W.; Wasson, J. R.; Hodgson, D. J.; Hatfield, W. E. *Inorg. Chem.* **1976**, *15*, 2107−2110.

(15) (a) Sarkar, B.; Ray, M. S.; Li, Y.-Z.; Song, Y.; Figuerola, A.; Ruiz, E.; Cirera, J.; Cano, J.; Ghosh, A. *Chem. - Eur. J.* **2007**, *13*, 9297−9309. (b) Tandon, S. S.; Thompson, L. K.; Manuel, M. E.; Bridson, J. N. *Inorg. Chem.* **1994**, *33*, 5555−5570. (c) Thompson, L. K.; Mandal, S. K.; Tandon, S. S.; Bridson, J. N.; Park, M. K. *Inorg. Chem.* **1996**, *35*, 3117−3125.

(16) (a) Ohba, S.; Kato, M.; Tokii, T.; Muto, Y.; Steward, O. W. *Mol. Cryst. Liq. Cryst. Sci. Technol., Sect. A* **1993**, *233*, 335−344. (b) Rodríguez-Fortea, A.; Alemany, P.; Alvarez, S.; Ruiz, E. *Chem. - Eur. J.* **2001**, *7*, 627−637.

(17) (a) Walsh, J. P. S.; Sproules, S.; Chilton, N. F.; Barra, A.-L.; Timco, G. A.; Collison, D.; McInnes, E. J. L.; Winpenny, R. E. P. *Inorg. Chem.* **2014**, *53*, 8464−8472. (b) Nanda, K. K.; Thompson, L. K.; Bridson, J. N.; Nag, K. *J. Chem. Soc., Chem. Commun.* **1994**, 1337−1338.

(18) Thompson, L. K.; Mandal, S. K.; Tandon, S. S.; Bridson, J. N.; Park, M. K. *Inorg. Chem.* **1996**, *35*, 3117−3125.

(19) (a) Law, N. A.; Kampf, J. W.; Pecoraro, V. L. *Inorg. Chim. Acta* **2000**, *297*, 252−264. (b) Gomez, V.; Corbella, M.; Roubeau, O.; Teat, S. J. *Dalton Trans.* **2011**, *40*, 11968−11975. (c) Escuer, A.; Aromí, G. *Eur. J. Inorg. Chem.* **2006**, *2006*, 4721−4736.

(20) (a) Berg, N.; Rajeshkumar, T.; Taylor, S. M.; Brechin, E. K.; Rajaraman, G.; Jones, L. F. *Chem. - Eur. J.* **2012**, *18*, 5906−5918. (b) Pantazis, D. A.; Krewald, V.; Orio, M.; Neese, F. *Dalton Trans.* **2010**, *39*, 4959−4967.

(21) (a) Gorun, S. M.; Lippard, S. J. *Inorg. Chem.* **1991**, *30*, 1625−1630. (b) Weihe, H.; Güdel, H. U. *J. Am. Chem. Soc.* **1997**, *119*, 6539−

6543. (c) Werner, R. D.; Ostrovsky, S.; Griesar, K.; Haase, W. *Inorg. Chim. Acta* **2001**, *326*, 78−88.

(22) (a) Le Gall, F.; Fabrizi de Biani, F.; Caneschi, A.; Cinelli, P.; Cornia, A.; Fabretti, A. C.; Gatteschi, D. *Inorg. Chim. Acta* **1997**, *262*, 123−132. (b) Hänninen, M. M.; Colacio, E.; Mota, A. J.; Sillanpää, R. *Eur. J. Inorg. Chem.* **2011**, *2011*, 1990−1996.

(23) (a) Puterová-Tokárová, Z.; Mrázová, V.; Kožíšek, J.; Valentová, J.; Vranovičová, B.; Boča, R. *Polyhedron* **2014**, *70*, 52−58. (b) Makohusová, M.; Mrázová, V.; Haase, W.; Boča, R. *Polyhedron* **2014**, *81*, 572−582.

(24) (a) Halcrow, M. A.; Sun, J.-S.; Huffman, J. C.; Christou, G. *Inorg. Chem.* **1995**, *34*, 4167−4177. (b) Clemente-Juan, J. M.; Chansou, B. T.; Donnadieu, B.; Tuchagues, J.-P. *Inorg. Chem.* **2000**, *39*, 5515−5519.

(25) Brechin, E. K.; Knapp, M. J.; Huffman, J. C.; Hendrickson, D. N.; Christou, G. *Inorg. Chim. Acta* **2000**, *297*, 389−399.

(26) (a) Bolcar, M. A.; Aubin, S. M. J.; Folting, K.; Hendrickson, D. N.; Christou, G. *Chem. Commun.* **1997**, 1485−1486. (b) Boskovic, C.; Brechin, E. K.; Streib, W. E.; Folting, K.; Hendrickson, D. N.; Christou, G. *Chem. Commun.* **2001**, 467−468. (c) Stamatatos, T. C.; Abboud, K. A.; Wernsdorfer, W.; Christou, G. *Polyhedron* **2007**, *26*, 2042−2046. (d) Taguchi, T.; Wernsdorfer, W.; Abboud, K. A.; Christou, G. *Inorg. Chem.* **2010**, *49*, 10579−10589.

(27) (a) Taguchi, T.; Daniels, M. R.; Abboud, K. A.; Christou, G. *Inorg. Chem.* **2009**, *48*, 9325−9335. (b) Canada-Vilalta, C.; Rumberger, E.; Brechin, E. K.; Wernsdorfer, W.; Folting, K.; Davidson, E. R.; Hendrickson, D. N.; Christou, G. *J. Chem. Soc., Dalton Trans.* **2002**, 4005−4010.

(28) Pech, L.; Bankovsky, Y. A.; Kemme, A.; Lejejs, J. *Acta Crystallogr., Sect. C: Cryst. Struct. Commun.* **1997**, *53*, 1043−1045.

(29) Taguchi, T.; Stamatatos, T. C.; Abboud, K. A.; Jones, C. M.; Poole, K. M.; O'Brien, T. A.; Christou, G. *Inorg. Chem.* **2008**, *47*, 4095−4108.

(30) See the Supporting Information.

(31) Anderson, P. W. *Phys. Rev.* **1950**, *79*, 350−356.

(32) Murray, K. S. *Coord. Chem. Rev.* **1974**, *12*, 1−35.

(33) Van Vleck, J. H. *The Theory of Electric and Magnetic Susceptibilities*; Oxford University Press: London, U.K., 1932.

(34) (a) O'Brien, T. A.; Davidson, E. R. *Int. J. Quantum Chem.* **2003**, *92*, 294−325. (b) Stamatatos, T. C.; Christou, A. G.; Mukherjee, S.; Poole, K. M.; Lampropoulos, C.; Abboud, K. A.; O'Brien, T. A.; Christou, G. *Inorg. Chem.* **2008**, *47*, 9021−9034. (c) Taguchi, T.; Stamatatos, T. C.; Abboud, K. A.; Jones, C. M.; Poole, K. M.; O'Brien, T. A.; Christou, G. *Inorg. Chem.* **2008**, *47*, 4095−4108.

(35) (a) Cauchy, T.; Ruiz, E.; Alvarez, S. *J. Am. Chem. Soc.* **2006**, *128*, 15722−15727. (b) Rudra, I.; Wu, Q.; Van Voorhis, T. *Inorg. Chem.* **2007**, *46*, 10539−10548. (c) Ruiz, E.; Rodríguez-Fortea, A.; Cano, J.; Alvarez, S. *J. Phys. Chem. Solids* **2004**, *65*, 799−803. (d) Carrasco, R.; Cano, J.; Mallah, T.; Jones, L. F.; Collison, D.; Brechin, E. K. *Inorg. Chem.* **2004**, *43*, 5410−5415.

(36) (a) Langley, S. K.; Chilton, N. F.; Moubaraki, B.; Murray, K. S. *Dalton Trans.* **2012**, *41*, 9789−9796. (b) Hamaguchi, T.; Doud, M. D.; Hilgar, J.; Rinehart, J. D.; Kubiak, C. P. *Dalton Trans.* **2016**, *45*, 2374−2377. (c) Moreno Pineda, E.; Chilton, N. F.; Tuna, F.; Winpenny, R. E. P.; McInnes, E. J. L. *Inorg. Chem.* **2015**, *54*, 5930−5941. (d) Canaj, A. B.; Tzimopoulos, D. I.; Siczek, M.; Lis, T.; Inglis, R.; Milios, C. J. *Inorg. Chem.* **2015**, *54*, 7089−7095.

(37) Bagai, R.; Abboud, K. A.; Christou, G. *Inorg. Chem.* **2007**, *46*, 5567−5575.

(38) Phillips, J. J.; Peralta, J. E.; Christou, G. *J. Chem. Theory Comput.* **2013**, *9*, 5585−5589.

(39) O'Brien, T. A.; O'Callaghan, B. J. *J. Chem. Theory Comput.* **2007**, *3*, 1275−1283.

(40) Ruiz, E.; Cano, J.; Alvarez, S. *Chem. - Eur. J.* **2005**, *11*, 4767−4771.

(41) Barra, A. L.; Gatteschi, D.; Sessoli, R. *Chem. Eur. J.* **2000**, *6*, 1608−1614.

(42) Chilton, N. F.; Anderson, R. P.; Turner, L. D.; Soncini, A.; Murray, K. S. *J. Comput. Chem.* **2013**, *34*, 1164−1175.

(43) *SHELXTL2013*; Bruker-AXS, Madison, WI, 2013.

(44) *SHELXTL2014*; Bruker-AXS: Madison, Wisconsin, USA, 2014.

(45) Davidson, E. R. *MAGNET*; Indiana University: Bloomington, IN, 1999.

(46) Kahn, O. *Molecular Magnetism*; VCH: New York, 1993.

(47) Bagai, R.; Datta, S.; Betancur-Rodriguez, A.; Abboud, K. A.; Hill, S.; Christou, G. *Inorg. Chem.* **2007**, *46*, 4535−4547.

(48) Gass, I. A.; Milios, C. J.; Collins, A.; White, F. J.; Budd, L.; Parsons, S.; Murrie, M.; Perlepes, S. P.; Brechin, E. K. *Dalton Trans.* **2008**, 2043−2053.

(49) Boskovic, C.; Sieber, A.; Chaboussant, G.; Güdel, H. U.; Ensling, J.; Wernsdorfer, W.; Neels, A.; Labat, G.; Stoeckli-Evans, H.; Janssen, S. *Inorg. Chem.* **2004**, *43*, 5053−5068.

(50) Boudalis, A. K.; Lalioti, N.; Spyroulias, G. A.; Raptopoulou, C. P.; Terzis, A.; Bousseksou, A.; Tangoulis, V.; Tuchagues, J.-P.; Perlepes, S. P. *Inorg. Chem.* **2002**, *41*, 6474−6487.

(51) Baca, S. G.; Filippova, I. G.; Keene, T. D.; Botezat, O.; Malaestean, I. L.; Stoeckli-Evans, H.; Kravtsov, V. C.; Chumacov, I.; Liu, S.-X.; Decurtins, S. *Eur. J. Inorg. Chem.* **2011**, *2011*, 356−367.